JOINT INSTITUTE FOR NUCLEAR RESEARCH

Veksler and Baldin Laboratory of High Energy Physics

FINAL REPORT ON THE START PROGRAMME

Detector Performance for Reduced Magnetic Field Configuration.

Supervisor

Dr. Vadim Kolesnikov

Student

Carlos Márquez

Universidad Autónoma Metropolitana

Participation period:

July 07 – August 26,

Summer Session 2024

August 24, 2024, Dubna, Moscow

Abstract

The MPD (Multi-Purpose Detector) experiment, located at the Nuclotron-based Ion Collider Facility (NICA) within the Joint Institute for Nuclear Research (JINR), aims to investigate heavy ion collisions within the energy range of $4\,\text{GeV} \leq \sqrt{s_{NN}} \leq 11\,\text{GeV}$. This study focuses on evaluating the performance of the Time Projection Chamber (TPC), a key tracking detector, under modified magnetic field conditions. Specifically, we examine the impact of reducing the magnetic field from 5 kG to 2 kG on the TPC's tracking efficiency and particle identification capabilities.

Our approach involves analyzing a dataset generated with both the full and reduced magnetic field conditions, comparing the effectiveness of different tracking cuts such as transverse momentum (p_T), Pseudorapidity (η), number of hits, and distance of closest approach (DCA). The study aims to determine how these modifications affect the TPC's ability to reconstruct particle tracks and identify primary and secondary particles accurately.

The methodology includes using custom-written software and macros to process and analyze large volumes of data on the JINR cluster. This analysis helps optimize the TPC's performance and adjust detection strategies for various magnetic field strengths. The results provide valuable insights into how changes in magnetic field strength influence detector efficiency and accuracy, thereby contributing to the overall effectiveness of the MPD experiment in studying high-density nuclear matter.

This report offers a comprehensive evaluation of the TPC under varying magnetic field conditions, with the goal of enhancing the precision and reliability of measurements in heavy ion collision experiments.

Keywords: MPD · TPC · Transverse momentum · Pseudorapidity · Magnetic Field

Contents

1 Introduction

The MPD (Multi-Purpose Detector) experiment is a pivotal undertaking in the realm of particle physics, housed within the Nuclotron-based Ion Collider Facility (NICA) at the Joint Institute for Nuclear Research (JINR). The experiment is specifically designed to probe the properties of nuclear matter under extreme conditions, particularly focusing on heavy ion collisions in an energy range of $4\,\text{GeV} \leq \sqrt{s_{NN}} \leq 11\,\text{GeV}$. This energy window is critical for studying the dense baryonic matter, a region of the quantum chromodynamics (QCD) phase diagram that remains largely uncharted. By investigating this uncharted territory, the MPD experiment seeks to provide new insights into the dynamics of hadrons and the mechanisms of particle production in a baryon-rich environment, addressing fundamental questions about the nature of matter at high densities.

The success of the MPD experiment relies heavily on its sophisticated array of detector systems, each meticulously designed to capture different aspects of the collision events. Central to this array is the Time Projection Chamber (TPC), the primary tracking detector that plays a vital role in recording the trajectories of charged particles produced in collisions. The TPC is tasked with providing high-resolution measurements of particle momentum, precise particle identification, and efficient separation of closely spaced tracks, all of which are essential for the comprehensive analysis of the collision data. The detector's performance is crucial in ensuring that the experiment meets its objectives, especially in the challenging environment of heavy ion collisions where particle multiplicity is extremely high.

This report is specifically focused on the TPC's performance under modified magnetic field conditions. In standard operating scenarios, the TPC functions within a magnetic field of 5 kG, which is necessary for achieving the high precision required for momentum resolution and particle identification. However, in this study, we explore the implications of reducing the magnetic field to 2 kG within the TPC. This reduction presents a unique opportunity to understand how changes in magnetic field strength affect the TPC's ability to maintain its critical functions. The decision to focus on the TPC is driven by its central role in tracking and identification, which are foundational to the success of the MPD experiment. By analyzing the TPC's performance under these adjusted conditions, we aim to identify any limitations or necessary adjustments to the analysis techniques, ensuring that the detector can continue to provide reliable data even with a reduced magnetic field.

Moreover, this investigation is practical implications for optimizing the MPD's performance under different operational constraints. Understanding how the TPC behaves with a lower magnetic field will inform decisions about detector settings and data analysis strategies, potentially leading to more efficient use of the detector in various experimental conditions. This study, therefore, represents a significant step in ensuring the robustness of the MPD experiment and its ability to deliver high-quality scientific results across a range of scenarios.

2 Theory

2.1 MPD Experiment

The MPD (Multi-Purpose Detector) experiment represents a significant endeavor in the realm of particle physics, situated as a spectrometer within the Nuclotron-based Ion Collider Facility (NICA) at the Joint Institute for Nuclear Research (JINR). Focused on studying heavy ion collisions within a specific energy range, ranging from $4\,\text{GeV} \leq \sqrt{s_{NN}} \leq 11\,\text{GeV}$, the MPD explores the high-density region of baryons, an area yet to be fully investigated. This experimental program aims to fill a gap in the energy scale, providing a deeper understanding of hadron dynamics and the production of multiple particles in a baryon-rich environment.

To achieve its objectives, the MPD relies on cutting-edge technology, including several key detector subsystems. The central barrel components exhibit an approximate cylindrical symmetry within $|\eta| < 1.5$, comprising the Time Projection Chamber (TPC), the Time of Flight Detector (TOF), and the Electromagnetic Calorimeter (ECal). The TPC serves as the main tracker, providing precise momentum measurements and particle identification, while the TOF identifies charged hadrons and offers precise time and coordinate measurements. The ECal, placed between the TOF and the MPD magnet, is crucial for detecting electromagnetic showers and plays a central role in photon and electron measurements. Additionally, the Fast Forward Detector (FFD) within the TPC barrel acts as a wake-up trigger, and the Forward Hadronic Calorimeter (FHCal) near the magnet end-caps helps determine collision centrality and the orientation of the reaction plane for collective flow studies.

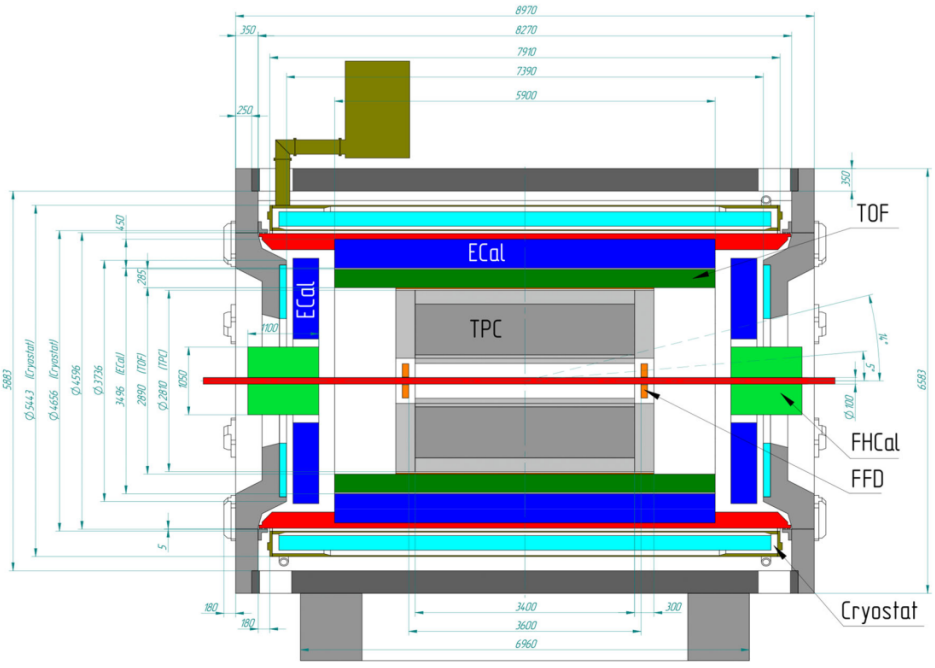

Figure 1: The overall schematic of the MPD subsystems in the first stage of operation (Stage 1) – cross-section by the vertical plane. [1]

This comprehensive setup, coupled with advanced software tools like MPDRoot specifically designed for this experiment, enables detailed event-by-event studies, providing crucial infor-

mation about trajectories, particle identification, and collision centrality. With its installation planned in two phases and the development of state-of-the-art detector subsystems, the MPD is poised to drive new discoveries and significantly contribute to advancing knowledge in this fascinating and ever-evolving field.

2.2 Time Projection Chamber

The MPD Time Projection Chamber (TPC) is the primary tracking detector within the central barrel. Along with the internal tracking system, time-of-flight system, and electromagnetic calorimeter, it ensures precise measurement of charged particle momentum, particle identification, vertex determination, two-track separation, and dE/dx measurement for hadronic and leptonic observables at pseudorapidities $|\eta| < 1.2$ and transverse momentum $p_T > 100 MeV/c$.

The electromagnetic calorimeter, in combination with TPC data, is crucial for reliable electron identification, especially for studying dielectron processes. The TPC must deliver high dE/dx resolution in the complex, high-multiplicity environment of central Au + Au collisions to achieve over 90% electron identification efficiency while rejecting pions at a ratio of 10^3 This information can be verified from the following source: [10].

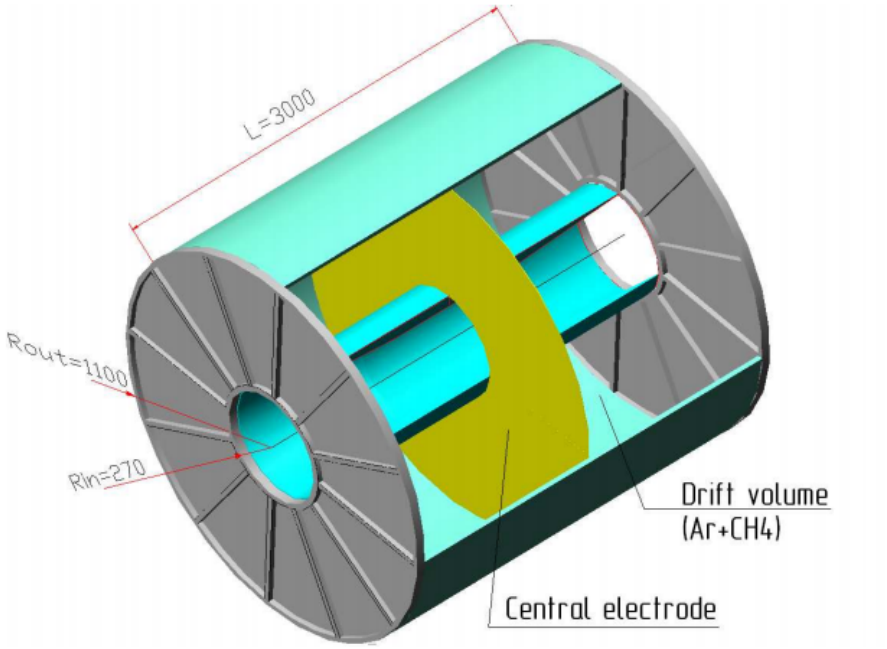

Figure 2: Schematic view of the MPD TPC. [11]

To maintain excellent momentum resolution and identification capabilities in this region, the TPC's end plate elements and associated readout electronics must be minimized for material budget, which currently stands at about 15%. The detector operates under a complete magnetic field of 5 kG in collider conditions. Key performance requirements for the TPC include efficient tracking up to $|\eta| < 1.2$, approximately 2% momentum resolution at 300 MeV/c transverse momentum, and a two-track resolution of about 1 cm for precise interference measurements.

2.3 Collider Mode of the MPD

The Collider for the MPD experiment is designed to operate in a fixed-energy mode, meaning that once the beam is injected, it is not further accelerated. This fixed energy configuration allows for precise control and measurement of heavy ion collisions under stable conditions.

2.3.1 Collider Configuration:

The Collider is housed within a specialized tunnel and includes additional infrastructure for two detectors and an electron cooler. It features two concentric collider rings situated vertically to facilitate beam superposition and separation. The distance between the median planes of the rings is 32 cm, achieved using dipole and quadrupole magnets with dual apertures in a single yoke.

The ring itself is shaped like a racetrack, consisting of two curved arcs and two long, straight sections. The minimum beta function at the interaction point is set at 35 cm, and the ring's acceptance is constrained by the aperture of the final focus lenses, which is not less than $40\,\pi\cdot$mm$\cdot$ mrad. The root mean square (rms) bunch length in collision mode is 60 cm, with an inter-bunch distance exceeding 21 meters. The arc's optical structure comprises 12 regular FODO-type cells, including focusing (QF) and defocusing (QD) quadrupoles, dipole magnets, and corrector packs.

2.3.2 Beam and RF Systems:

To manage beam storage and bunch formation, the Collider employs three independent radiofrequency (RF) systems:

1. RF Barrier Bucket System (RF1): Operates at a voltage amplitude of 5 kV to store the required beam intensity.

2. First Narrow-Band RF System (RF2): Functions at harmonics of the revolution frequency corresponding to the bunch number, with a maximum voltage amplitude of 100 kV. It handles beam bunching and compression.

3. Second Narrow-Band RF System (RF3): Operates at harmonics three times greater than the first system, providing a maximum voltage amplitude of 1 MV to achieve the necessary bunch length for collision experiments.

2.3.3 Injection and Cooling Systems:

The Collider's injection system includes a septum (MS) and a kicker (K), located in a "missing" dipole cell of the bending arc. The emittance of the injected beam from the Nuclotron is $\epsilon_{x,y} = 1.2\,\pi \cdot \text{mm} \cdot \text{mrad}$.

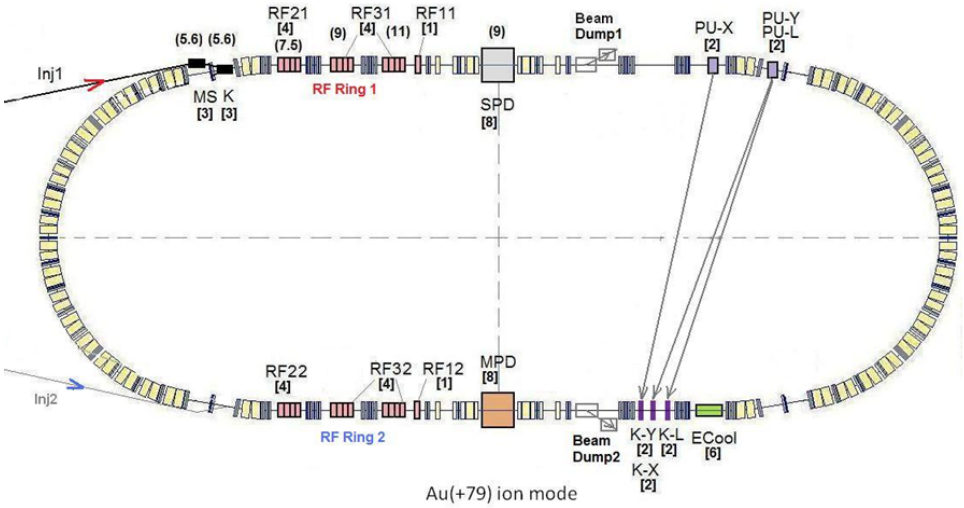

Figure 3: Scheme of the collider ring with equipment and insertions.[10]

For maintaining luminosity during heavy ion collisions, the Collider utilizes both electron and stochastic cooling systems. The electron cooling system operates in the ion energy range of 1 to 3 GeV/u, while the stochastic cooling system, which operates from 2 to 4 GHz, is used from 3 to 4.5 GeV/u. The stochastic cooling system includes horizontal, vertical, and longitudinal pick-ups (PU-X, PU-Y, PU-L) and corresponding kickers (K-X, K-Y, K-L). The longitudinal cooling is achieved using the Palmer method.

This configuration ensures that the Collider can maintain high luminosity and precise control over the beam conditions, crucial for conducting accurate and high-resolution experiments in heavy ion collisions.

2.4 Reduced Magnetic Field

The importance of studying what happens to the collision mode when the magnetic field is reduced lies in the fact that the way we reconstruct particles is based on the trajectory formed by the transverse momentum when interacting with the magnetic field. In other words, thanks to the magnetic field, we can correctly reconstruct particles through their transverse momentum.

However, there are particles with low transverse momentum that, even with the full magnetic field (Bz = 5 kG), are not significantly affected. These particles are trapped rotating within the Time Projection Chamber (TPC), preventing them from reaching the detector limits and, therefore, they cannot reach other detectors.

This situation makes it difficult to accurately reconstruct this type of particle with low transverse momentum. Since we want to reconstruct and record all particles, we seek to reduce the magnetic field to evaluate if we can thus improve the reconstruction of these particles.

It should be noted that this study is only analyzing the case of a reduced magnetic field in the TPC. However, studies will also be conducted where the magnetic field will be increased by a factor of 2, with the aim of exploring all possible scenarios.

2.5 MPDRoot

MPDRoot is a specific implementation for the MPD experiment in NICA. It is built on Root and FairRoot, adapting the general functionalities of these frameworks to the particular needs of the MPD experiment. MPDRoot provides specialized tools for data analysis of the MPD experiment, including event reconstruction algorithms, data filtering techniques and results visualization. Its integration with Root and FairRoot ensures seamless interoperability with other analysis tools and allows effective collaboration between different research groups.

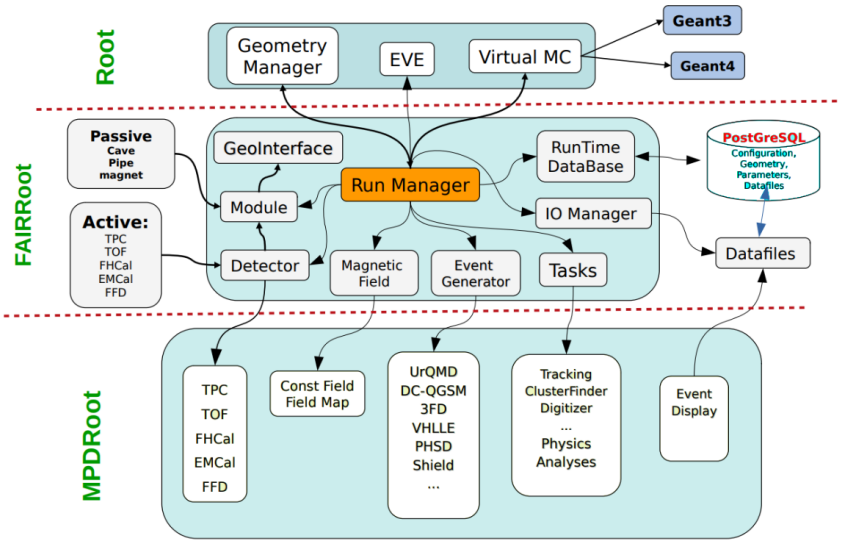

Figure 4: Architecture of MPDRoot. [2]

3 Project "Collider Mode: Reduced Magnetic Field"

This activity is made up of two tasks that complement each other. Task 1 is the one discussed in this report. However, my colleague physicist Alejandro San Juan López is responsible for developing the objectives of task 2 [1].

1. **Task 1:** Primary vertex determination and Particle Track reconstruction, optimization of cuts in η, p_T, number of hits on TPC.

2. **Task 2.** Particle identification determination of spectra using information about the energy losses (dE/dx) in the TPC and the Time-of-flight from the TOF detector.

3.1 Task 1: Primary vertex determination and Particle Track reconstruction, optimization of cuts in η, p_T, number of hits on TPC.

Task 1 Objetives

i . Get Track reconstruction efficiency as a function of the transverse momentum p_T of track, for primary and secondaries.

[1] If you want to know how task 2 was done, you can read my colleague's work or review his work on GitHub. `https://start.jinr.ru/index.php?session_id=5`

ii . Get Relative Transverse momentum resolution for primary tracks for the phase space (η and p_T) available for TPC.

iii . Comparison of results with default magnetic field.

4 Approach to the Task of Analysis

Before starting the development of the task, we need to understand each of the concepts we will be working with. This understanding will help us propose more effective cuts and achieve better optimization.

4.1 Information to Analysis

For this analysis, it is proposed that the magnetic field be reduced from $B = 5$ kG to $B = 2$ kG in the TPC. That is to say that new information is generated under this condition. Which, is:

Data Set: Available resources at ICN cluster

	Request 25	Request 28
Collision system	Bi + Bi @9.2GeV	Bi + Bi @9.2GeV
Event Generator	UrQMD	UrQMD
Production	50 Million Events	10 Million Events
Magnetic Field	5 kG	2 kG

Table 1: Comparison table between the difference of Request 28 and Request 25.

For request 25, we have a production of 50 million events, only for the comparison in this part only 5 million were used.

For the reduced magnetic field is request 28, for the complete magnetic field is request 25. The cuts for when you have the full magnetic field are already known, which are as follows:

Variable	Cut
Transverse momentum	$p_T > 0.1$ (GeV/c)
Pseudorapidity	$\eta \in (-1, 1)$
Number of Hits	Number of Hits > 16
DCA Global	DCA Global > 0.5 cm

Table 2: Cuts for the Full Magnetic Field.

The purpose to help us with this is to find out what difference there is when the magnetic field is reduced and why this happens. That is, as we get this information we will replicate the already known cuts for the full magnetic field. Where we compare each and see how efficient these new cuts are or if they need to be changed.

Of course, this is what is mentioned as the final step of our task, only that it is necessary to go comparing each cut as they are made so you can have a better clarity when making new cuts.

Clearly these cuts are also applied to the cuts that exist for primary and secondary particles.

4.2 Variables

Here, we provide a detailed explanation of each variable involved in setting the necessary criteria for our analysis. Understanding these variables is crucial for accurately defining the cut values and optimizing the performance of the detector.

4.2.1 Transverse momentum

Transverse momentum distributions are the distributions of the hadron's quark or gluon momentum a that are perpendicular to the momentum transfer between the beam and the hadron. Specifically, they are probability distributions to find inside the hadron a parton with a transverse momentum p_T and longitudinal momentum fraction x.

Transverse Momentum Resolution

As already mentioned in the theoretical part, the transverse momentum is important for the reconstructed of particles in the detector. That is why we will calculate and plot the resolution of the transverse momentum.

To calculate the transverse momentum response, we will use the following equation:

$$\Delta p_T = \frac{|p_T^{reco} - p_T^{MC}|}{p_T^{MC}} \tag{1}$$

By obtaining the resolution of the transverse momentum, and plotting it against the pseudorapidity or other variables. We can get and see how the signal is cleaned of the reconstructed particles. Although in this report we will mainly focus only on the histogram of the resolution of the histogram against pseudorapidity.

4.2.2 Pseudorapidity

Pseudorapidity is an approximation to Rapidity. This quantity is sometimes used instead of Rapidity as it is easily calculated from the cartesian angle between the particle direction above or below the beam line and has a direct relationship with detector components. This quantity is precisely equivalent to Rapidity for massless particles.

$$\eta = \frac{1}{2} ln \left(\frac{|\mathbf{p}| + p_Z}{|\mathbf{p}| - p_Z} \right) \tag{2}$$

This equation is an theoretical approximation, but when we use in our analysis we need to make a little correction, that's means:

$$\eta = \frac{1}{2} ln \left(\frac{|\mathbf{p}| + p_Z}{|\mathbf{p}| - p_Z + 1.0 \times 10^{-13}} \right) \tag{3}$$

This small correction will help us to avoid that in the lower part it becomes zero in the case the particle be parallel to beam axis and thus to avoid that one has an indetermination in our equation. The code for the analysis can be found on GitHub, in line 467 [2].

[2]You can check it at the following link, `https://github.com/iamaldonado/START_Summer24/blob/main/CarlosMarquez/lowMgF/lowMgF.cxx`

The value we use is 1.0×10^{-13}, it's an dimensionless value and the value was arbitrary, since the only condition is that it's a very small value.

4.2.3 DCA: Distance of Closest Approach

The distance of closest approach of two objects is the distance between their centers when they are externally tangent. The objects may be geometric shapes or physical particles with well-defined boundaries. The distance of closest approach is sometimes referred to as the contact distance. The figure 5 shows an example of this variable for secondary particles produced by the decay of a V0 particle.

$$DCA_{Global} = \sqrt{DCA_X^2 + DCA_Y^2 + DCA_Z^2} \tag{4}$$

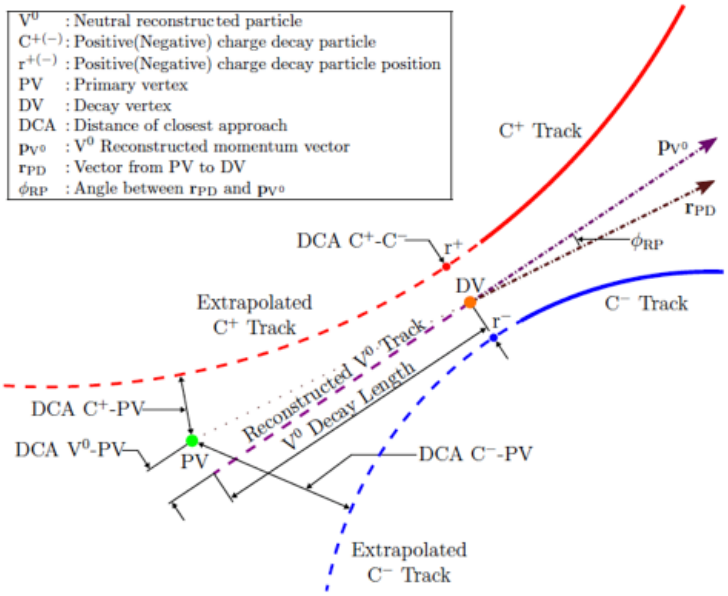

Figure 5: Scheme of V0 decay in which is possible to appreciate the DCA of the tracks of secondary particles to primary vertex.[3]

4.2.4 Primary Vertex

Primary vertex has position and time. Primary particle has a particle ID, momentum and optionally polarization. One or more primary particles may be associated with a primary vertex. One event may have one or more primary vertices.

Primary Vertex Resolution

The resolution of the primary vertex as opposed to the resolution does not need to be divided between the Monte Carlo primary vertex, since we are only interested in studying the difference of the primary vertex. And if we do the division then we get very small values. For the collider mode, we have a real distribution of the primary vertex.

$$\Delta Z = |Z_{reco} - Z_{MC}| \tag{5}$$

4.2.5 Primary particles

Primary particles are fundamental entities that emerge directly from the collision or interaction of high-energy particles, such as protons or heavy ions, in particle physics experiments. These collisions can occur in accelerators or in natural cosmic ray interactions with the Earth's atmosphere.

In the context of particle physics simulations, primary particles encompass not only the directly produced particles resulting from the collision but also any particles generated by the event generator software. Event generators simulate the entire collision process, from the initial collision to the final-state particles produced in the interaction.

4.2.6 Secondary particles

Secondary particles can be generate in both from within the primary particles themselves and from interactions with detector materials.

Decay Products of Primary Particles: Inside primary particles like lambdas (Λ) and (κ), which possess properties such as strangeness, decay processes can occur even before the particles reach a detector. These decays result in the production of secondary particles such as protons (p) or pions (π). This process contributes to the formation of secondary particles without the need for external interactions with the detector.

We will use the Mother ID to identify the primary particles, where we will have the following conditions for each.

$$\text{Primary particles: Mother ID} = 1.$$

$$\text{Secondary particles: Mother ID} \neq 1$$

4.3 Efficiency of the Transverse Momentum

When we have the cuts, we see the Efficiency of the Transverse momentum to see how efficiency are the cuts that we made. To obtain this, we divide the distributions of the transverse momentum reconstructed between the transverse momentum Monte Carlo.

$$Efficiency = \frac{p_T^{RECO}}{p_T^{MC}} \tag{6}$$

5 Results

At least 3 objectives were mentioned in the list of objectives for the task. However, several steps were taken to carry out the analysis and it may appear that some objectives are being mixed. So you will go explaining how things were obtained so that the reader is not lost and can be as clear as possible.

5.1 First Steps

Our study begins by tracing the distributions of the momentum transverse against Pseudorapidity. When doing the reconstruction 6(b) and the Monte Carlo 6(a), we can observe in part of the reconstruction many particles on top that are being generated and may be by contact with some detector or a subsequent decay. This information is just noise, as it does not help us to know what is happening in our collision under these conditions.

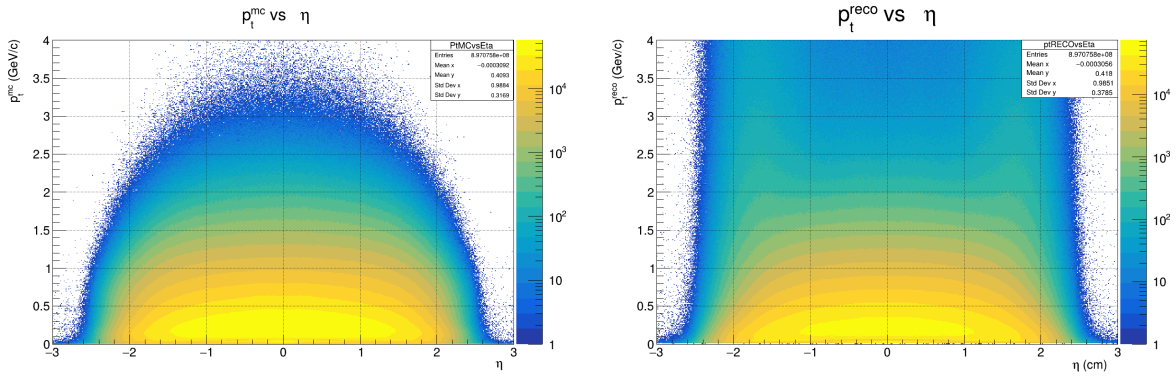

(a) Δp_T^{MC} vs η without cut.

(b) Δp_T^{MC} vs η with cut in Number of Hits.

Figure 6: Momentum Transverse vs Pseudorapidity.

In principle, when looking at the transverse reconstructed momentum distribution, there are many particles that are being reconstructed above three that do not appear in the Monte Carlo transverse momentum distribution. So it may be a good start for our analysis.

5.2 First cut in Number of Hits

The first cut was made in the number of Hits. To see the comparison more clearly, it will be plotted with and without cut to see the comparison in a clearer way.

The first cut was not so complicated to study, if we see in the histogram 7(a), in the red line the errors are very high, and if we make a cut like in the full magnetic field, it would lead to an error rate greater than 60%, so it was decided to cut the number of hits to 27. Allowing in this way to have a 20% error rate in our reconstructed particles.

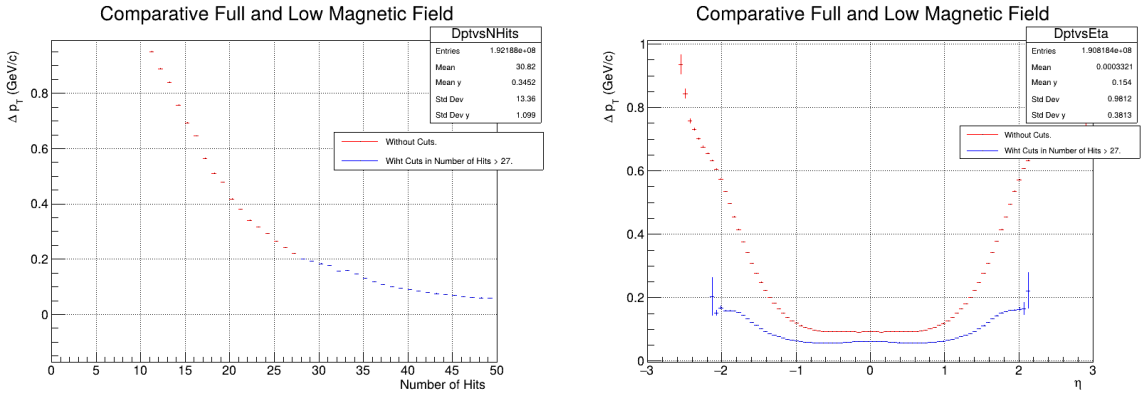

(a) Comparative of Δp_T vs Number of Hits with and without cuts Number of Hits.

(b) Comparative of Δp_T vs η cuts Number of Hits and cut in Number of Hits.

Figure 7: Comparative with and without cuts in the Number of Hits.

Now we see figure 7(b), in which we have the histogram of the resolution distribution of the transverse momentum against the pseudorapidity and observe that after the cut (blue line). There is a significant improvement in what we are getting. However, we still have points with very large error rates. So now we will see where to make the cut in the pseudorapidity.

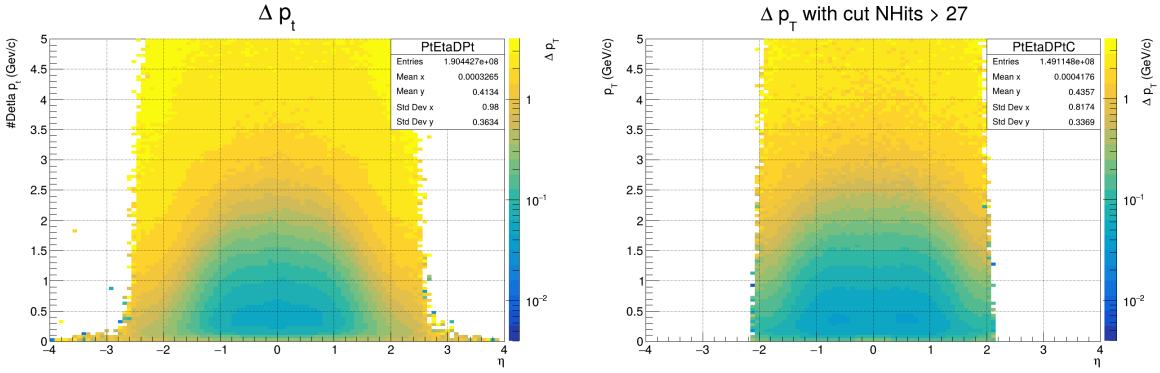

(a) The Δp_T without cut.

(b) The Δp_T with cut in Number of Hits.

Figure 8: Comparative with and without cuts in the Number of Hits.

Comparing both histograms of the resolution of the transverse momentum, it is clear how the signal has been cleaned. Because much of the periphery of the pseudorapidity has disappeared, which is something we were looking for since it is only noise.

5.3 Cut in Pseudorapidity

To evaluate where we could make a cut, it was sufficient to review the histograms with the cut on the number of hits. These histograms are found in the previous subsection. By focusing on pseudorapidity with the cut, we can zoom in slightly and determine where an optimal cut could be made. Upon doing this, it was observed that the best cut is in the range of -1.5 to 1.5 for pseudorapidity, which allows us to have an error of less than 10% in particle detection.

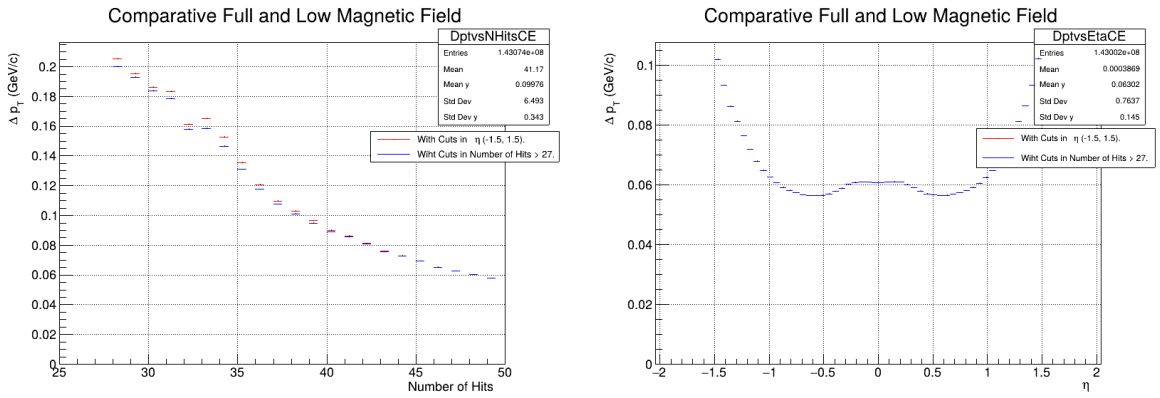

(a) Comparative of Δp_T vs Number of Hits with cuts Number of Hits and with cut in η.

(b) Comparative of Δp_T vs η with cuts Number of Hits and with cut in η.

Figure 9: Comparative with cut in Number of Hits and with cuts in η.

If we look at the histograms in Figure 28, we can see that for pseudorapidity, the error is confirmed to be less than 10%, which is positive for the optimization we are aiming for. However, if we now examine the distribution of the number of hits, there is a slight improvement.

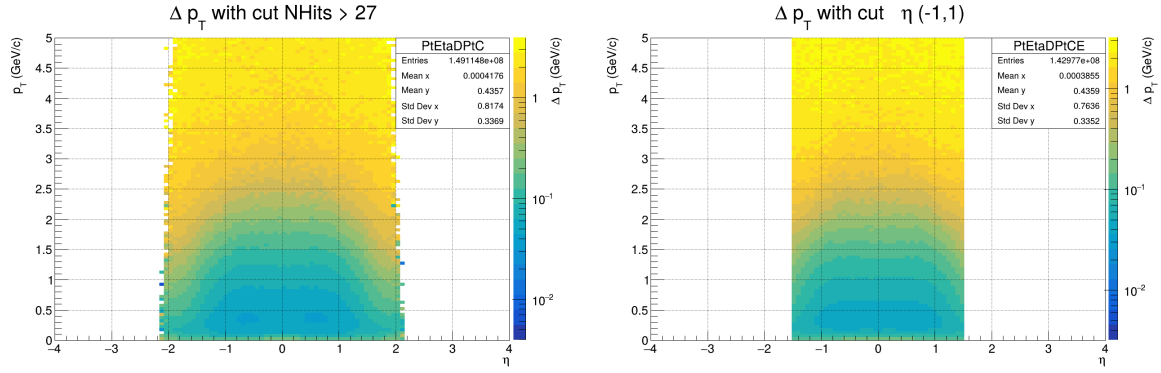

(a) The Δp_T with cut in Number of Hits.

(b) The Δp_T with cut in η.

Figure 10: Comparative with cut in Number of Hits and with cuts in η.

Once again, by comparing both histograms of the transverse momentum resolution, it is clear how the signal has been cleaned up. Now, the peripheral part of the pseudorapidity has been cleaned more homogeneously. However, there is still a significant amount of noise in the upper part above 2 in the vertex of the transverse momentum resolution. Nevertheless, we can see how the signal continues to be cleaned up with the remaining cuts.

5.4 Cut on the DCA Global

Determining the cut for the Global DCA was not as straightforward as the previous cuts. We will not display all the histograms that were created to determine the cut. In summary, the Global DCA distributions were obtained, calculated using formula 2. This distribution was obtained for all particles, for primary particles, and for secondary particles. This gave us a preliminary

idea of where the cut could be made, but to verify this, we divided the Global DCA distribution of primary particles by that of secondary particles, as well as the Global DCA distribution of primary particles by all particles, and similarly for secondary particles.

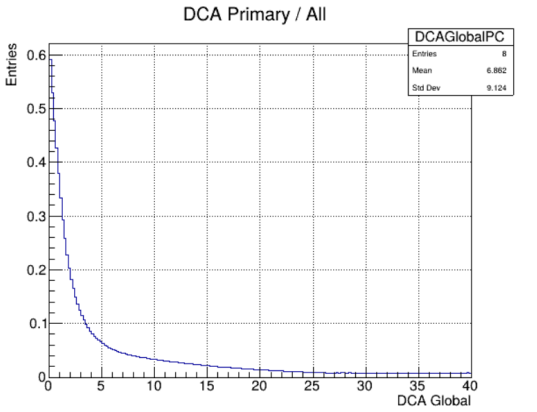

(a) Division of the distribution of DCA Global primary particles among the distribution of all particles.

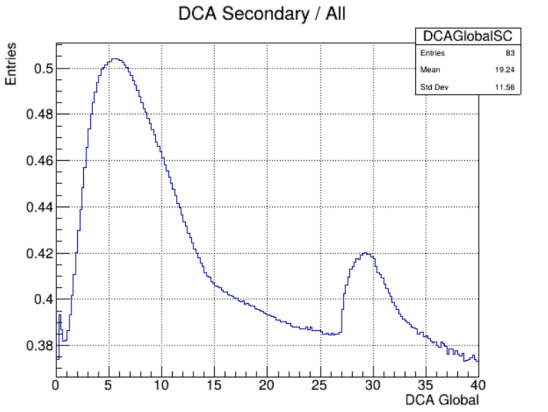

(b) Division of the distribution of DCA Global secondary particles among the distribution of all particles.

Figure 11: Division of the distribution of DCA Global.

These histograms can be seen in Figure 11. The histogram of primary particles relative to all particles doesn't provide much information for the cut, but the histogram of secondary particles relative to all shows the distribution of secondary particles more clearly.

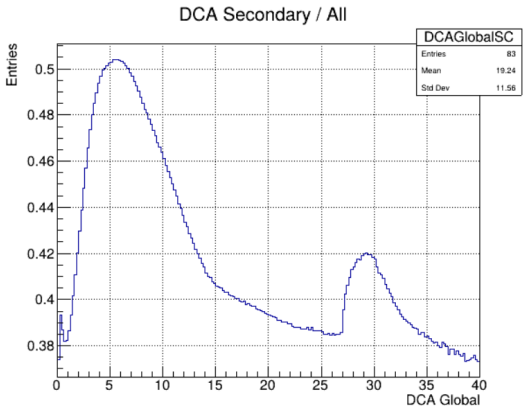

(a) Division of the distribution of DCA Global secondary particles among the distribution of all particles.

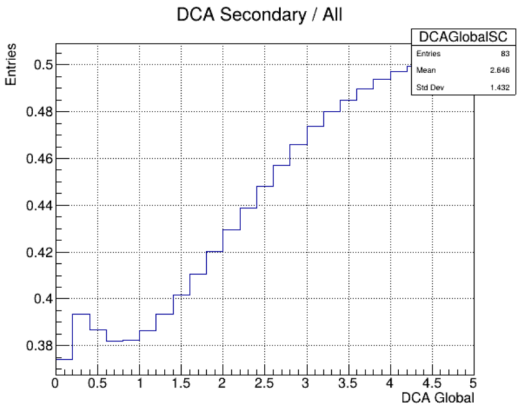

(b) Zoom to Division of the distribution of DCA Global secondary particles among the distribution of all particles.

Figure 12: Division od the distribution of DCA Global for Secondary Particles.

By zooming in on this section, we can identify a suitable cut point for the Global DCA parameter, which could be set at 1 cm. This would help us achieve a 30% error margin in the Global DCA variable.

5.5 Cut on the Vertex Position

For the cut in primary vertex had to make last minute corrections. Because the resolution that was being calculated was wrong. Since it was all divided between the Z Monte Carlo. And as already explained in the theoretical part, that is wrong. So we made the correction.

However, we are working with 10 million events. Only that in cluster at the dates when the report is being written it is saturated. So we could only run less than 1 million events. Due to lack of time, we will only work with these data here, but it is expected that in the near future the analysis will be done with all events.

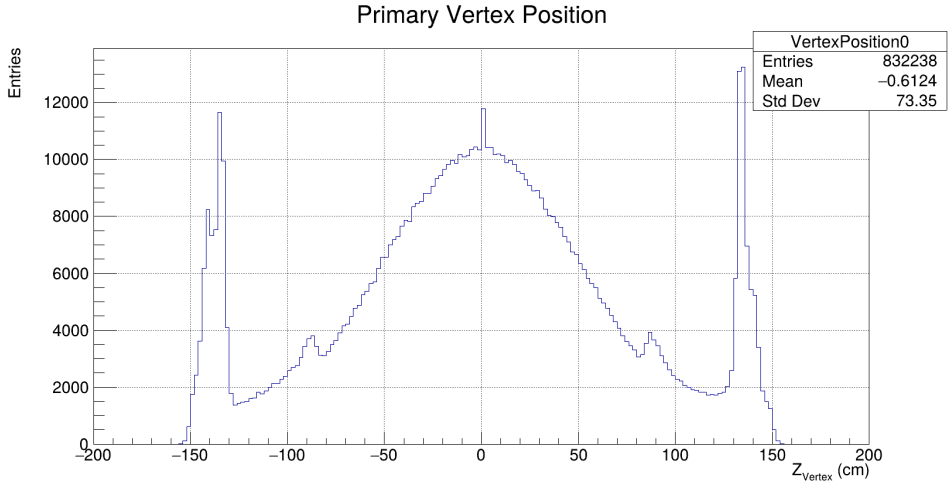

Figure 13: Primary Vertex Position Distribution.

In Figure 13, which shows the distribution of the primary vertex position, we might initially consider a cut in the range of -110 to 110. However, two peaks around -80 and 80 suggest that this initial cut is not adequate. Therefore, several histograms were created to help find a more suitable cut.

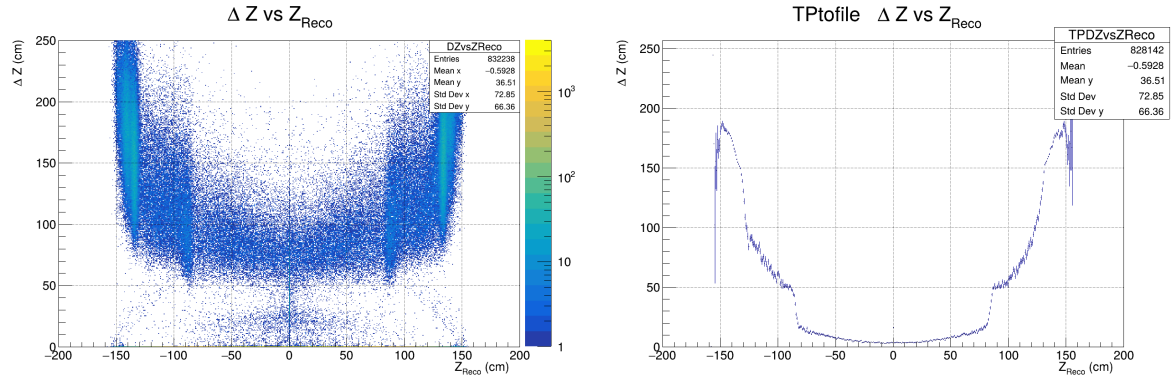

(a) Resolution of the Primary Vertex versus Primary Vertex on Z.

(b) TProfile of the Resolution of the Primary Vertex versus Primary Vertex on Z.

Figure 14: Resolution of the Primary Vertex versus Primary Vertex on Z.

In Figure 14, which shows the Resolution of the Primary Vertex versus the Primary Vertex position on Z, we observe an almost symmetrical figure, which is expected in collider mode. In

Figure 14a, there is a very thin yellow band with over 10^3 events, which is considerably higher compared to what appears at -150 and 150. On the vertical axis, representing the primary vertex resolution, there are very few events above 50 cm.

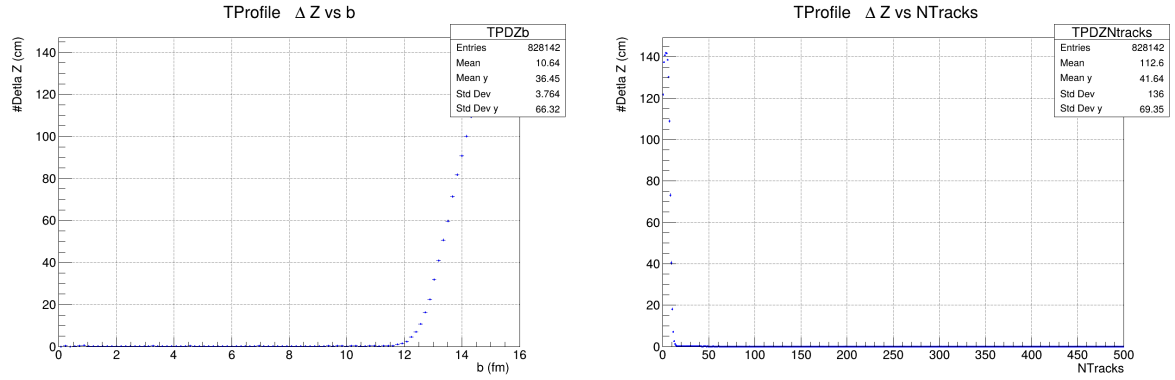

(a) TProfile of the Resolution of the Primary Vertex versus the Impact Parameter.

(b) TProfile of the Resolution of the Primary Vertex versus the Number of Tracks.

Figure 15: TProfile of the Resolution of the Primary Vertex vs Different Parameters.

In Figure 15a, it is observed that for peripheral events, the parameter b should be greater than 12 fm (indicating low multiplicity), leading to an increased error in primary vertex reconstruction. Figure 15b indicates that if the number of tracks is small (in peripheral collisions), the resolution tends to increase its error.

5.6 Comparative between the Full Magnetic Field and Reduced Magnetic Field

Now, we will compare the cuts obtained for the reduced magnetic field with those existing for the full magnetic field. Starting with the first cut, which was in the number of hits, in our case, the cut is at 27, whereas for the full magnetic field, it is at 16. Looking at Figure 16a, we notice that the error is about 20%. This indicates that similar cleanliness is achieved in both cases. The same occurs when this cut is applied to the pseudorapidity distribution.

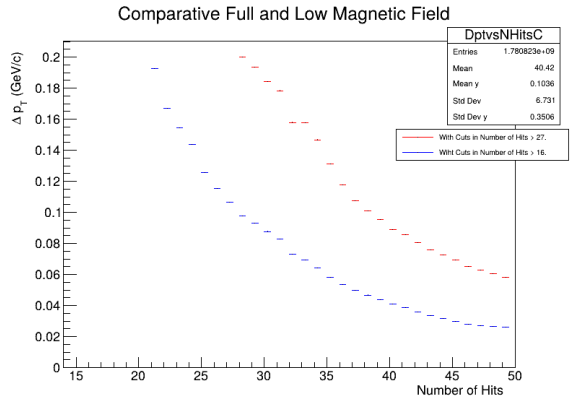

(a) Comparative Full and Reduce Magnetic Field with cut in Number of Hits.

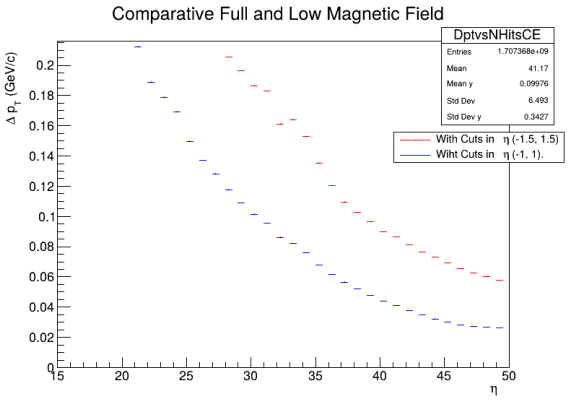

(b) Comparative Full and Reduced Magnetic Field with cut in η.

Figure 16: Comparative Full and Reduced Magnetic Full cuts on the distributions of Number of Hits.

For the second cut, which is pseudorapidity, we see that in our case, there is a 10% error. However, for the full magnetic field, the error is less than 5%. Therefore, a more effective way to optimize this cut would be to recreate these histograms, comparing the information from both cases using the same histograms.

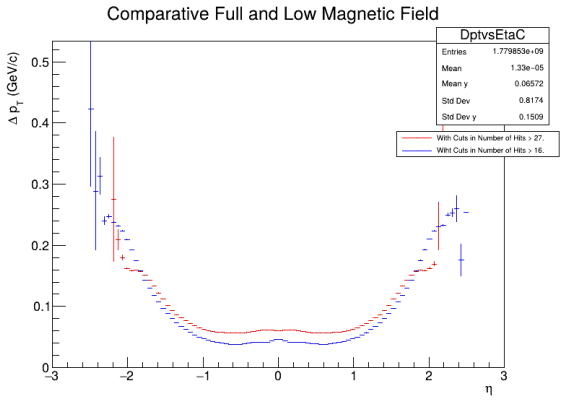

(a) Comparative Full and Reduced Magnetic Field with cut in Number of Hits.

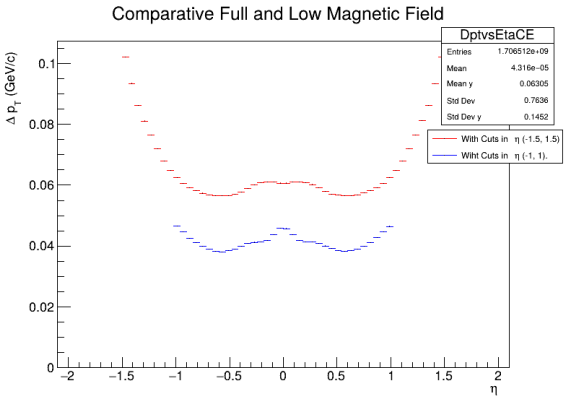

(b) Comparative Full and Reduced Magnetic Field with cut in η.

Figure 17: Comparative Full and Reduced Magnetic Full cuts on the distributions of η.

We now analyze the distributions of transverse momentum resolution versus Global DCA, starting with the distribution of all particles (Figure 18). Initially, we observe that for our cut, a trend appears at 1.5 in Global DCA, with a 12% margin of error. This differs from the full magnetic field, which shows this trend at 3 in Global DCA and with a margin of error below 16

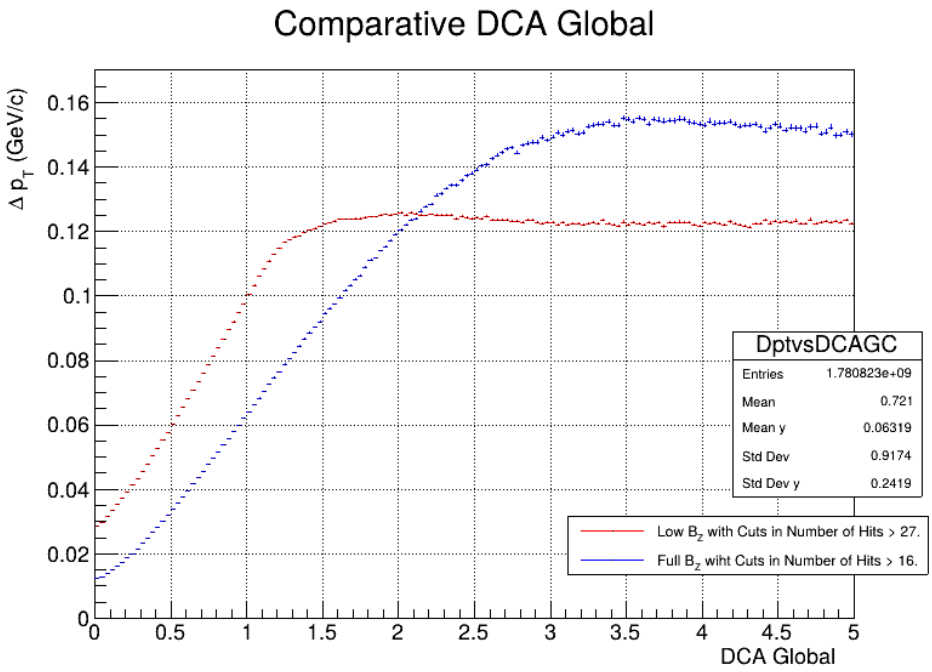

Figure 18: Comparative Full and Reduced Magnetic Full cuts on the distributions of DCA Global.

For primary particles (Figure 19a), there is a difference, as no clear trend is observed in the reduced magnetic field, unlike in the full magnetic field, where the same behavior seen in Figure 18 is present. This contrasts with secondary particles (Figure 19b), where a trend similar to that in Figure 18 is observed in both cases.

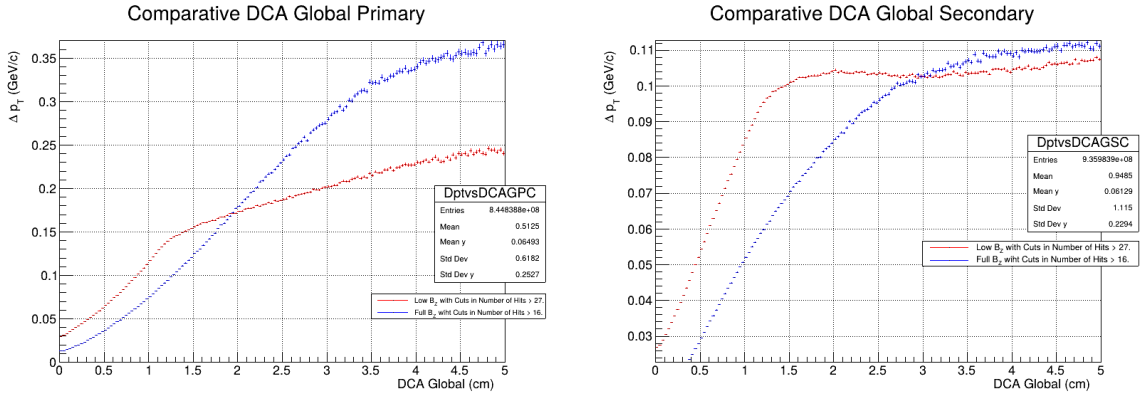

(a) Comparative Full and Reduced Magnetic Full cuts on the distributions of DCA Global Primary.

(b) Comparative Full and Reduced Magnetic Full cuts on the distributions of DCA Global Secondary

Figure 19: Comparative Full and Reduced Magnetic Full cuts on the distributions of DCA Global.

As seen in Figures 18 and 19, this analysis is done with only the hit count cut. It remains to examine how the distributions behave when the other cuts are applied. However, due to time constraints and the issue mentioned in the "Primary Vertex Cut" section related to the cluster, it was not possible to fully analyze these cuts. Nonetheless, this analysis is expected to continue in future work.

In the final part, transverse momentum resolution is compared against pseudorapidity for each of the cuts. Again, due to the previously mentioned issue, it was not possible to compare all cuts, as not all events could be processed for both the full and reduced magnetic fields.

However, when comparing both cases, clear trends are observed in how these distributions are being optimized.

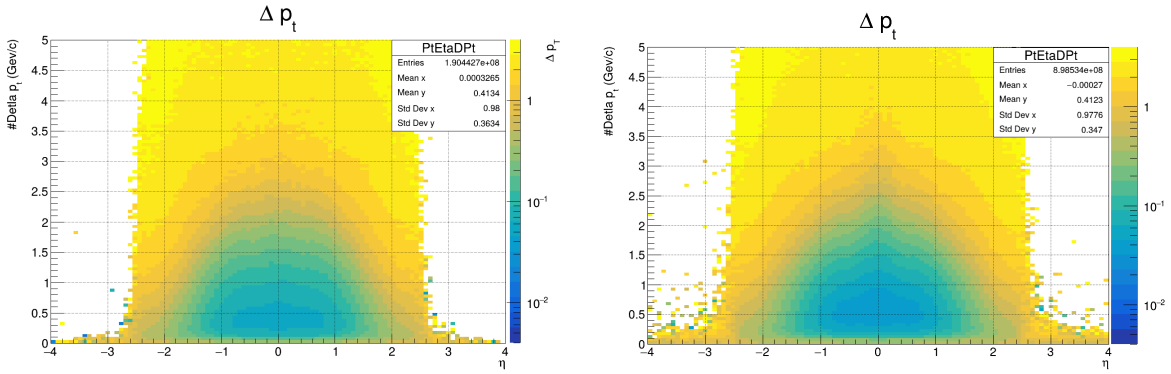

(a) The Δp_T without cut for Reduce Magnetic Field. (b) The Δp_T without cut for Full Magnetic Field.

Figure 20: Comparative without cuts for Full and Reduced Magnetic Field.

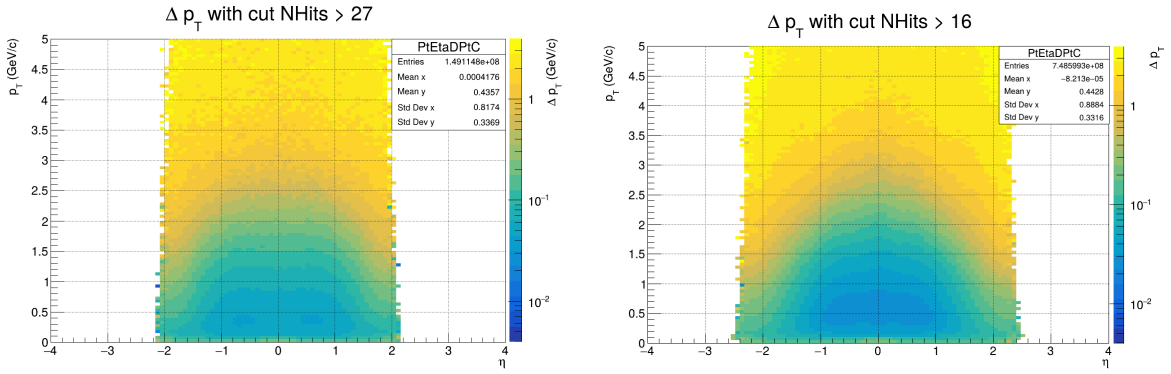

(a) The Δp_T with cut in Number of Hits for Reduce Magnetic Field. (b) The Δp_T with cut in Number of Hits for Full Magnetic Field.

Figure 21: Comparative with cuts in Number of Hits for Full and Reduce Magnetic Field.

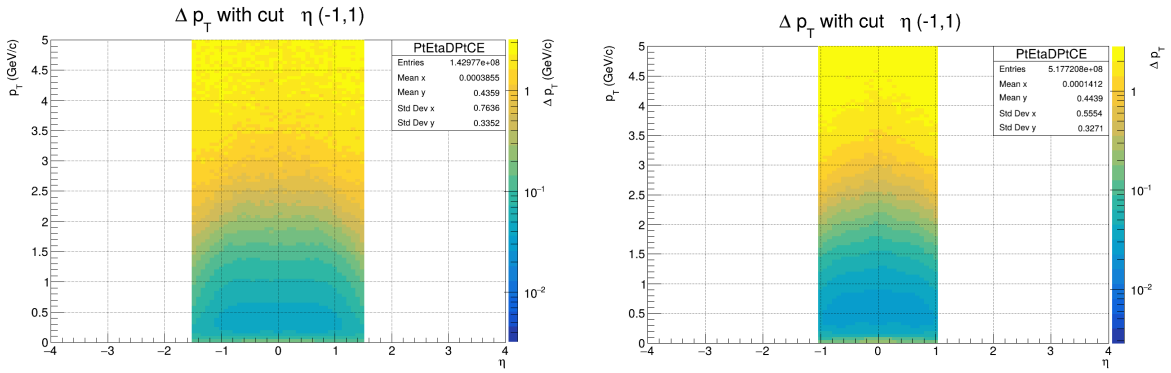

(a) The Δp_T with cut in η for Reduce Magnetic Field. (b) The Δp_T with cut in η for Full Magnetic Field.

Figure 22: Comparative with cuts in η for Full and Reduce Magnetic Field.

One notable observation is that for the reduced magnetic field, on the upper part of the vertical axis, above 2, noise starts to appear, meaning information that is not useful for analysis. In contrast, for the full magnetic field, this limit may be slightly above 2. However, no definitive conclusion can be drawn as the available data for both configurations has not been fully analyzed. It is hoped that this will be corrected in future work.

5.7 New Cuts for Reduce Magnetic Field

After all this analysis, we can conclude that the cuts for a reduced magnetic field are as follows:

Variable	Cut
Transverse momentum	$p_T > 0.1$ (GeV/c)
Pseudorapidity	$\eta \in (-1.5, 1.5)$
Number of Hits	Number of Hits > 16
DCA Global	DCA Global > 0.5 cm
Primary Vertex Position	Vtx $\in (-50, 50)$

Table 3: Cuts for the Reduced Magnetic Field.

We will evaluate these cuts by determining the efficiency of the transverse momentum resolution. This will enable us to assess how optimal these cuts are for the scenario of a reduced magnetic field. However, as this analysis is ongoing, any cuts that are found to be suboptimal will be refined and improved over time.

5.8 Efficiency of the Transverse momentum

Now with these cuts, we see the efficiency of the transverse momentum. For this we already mentioned that we must divide the distributions of the reconstructed transverse momentum between the Monte Carlo transversal momentum. For both cases we must apply these cuts, but only for the case of transverse reconstructed momentum we will apply all the cuts.

Variable	Cut
Transverse momentum	$p_T > 0.1$ (GeV/c)
Pseudorapidity	$\eta \in (-1, 1)$
Number of Hits	Number of Hits > 16
DCA Global	DCA Global > 0.5 cm
Primary Vertex Position	Vtx $\in (-50, 50)$

Table 4: Cuts made in the transverse momentum distributions reconstructed

For the case of transverse Monte Carlo momentum, it is not necessary to apply all the cuts, since some are totally inappropriate when working with Monte Carlo simulation. The applied cuts are:

Variable	Cut
Transverse momentum	$p_T > 0.1$ (GeV/c)
Pseudorapidity	$\eta \in (-1, 1)$
Primary Vertex Position	Vtx $\in (-50, 50)$

Table 5: Cuts made in the transverse momentum distributions Monte Carlo

Once again, in the case of the full magnetic field, not all data was processed, so only a small sample was analyzed. Nevertheless, it was not necessary to analyze all events, as the trend is clear in both cases, and they appear to be very similar.

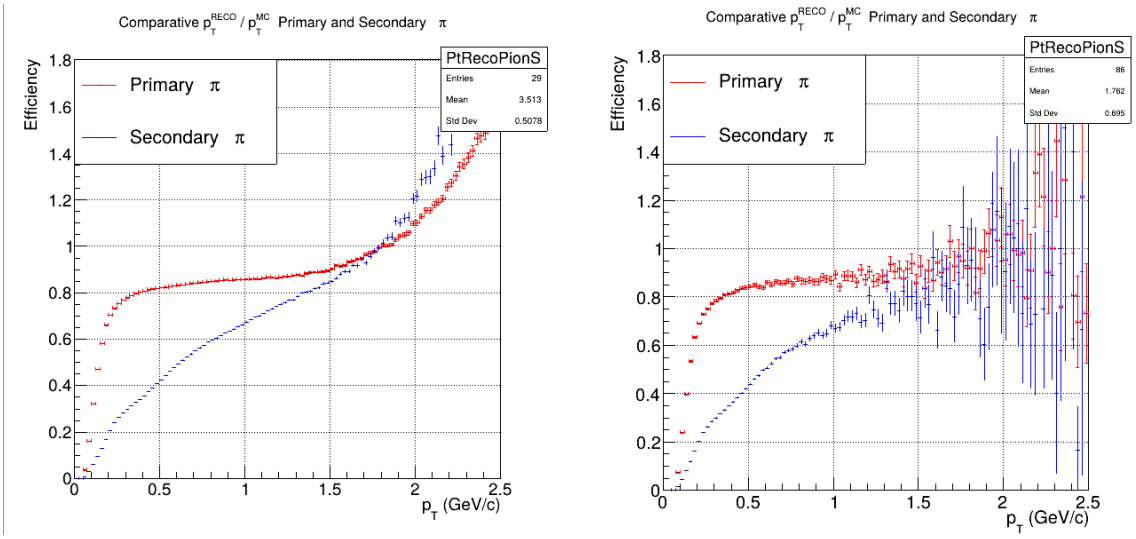

(a) The Δp_T with cut in Number of Hits.

(b) The Δp_T with cut in η.

Figure 23: Comparative with and without cuts of the Δp_T.

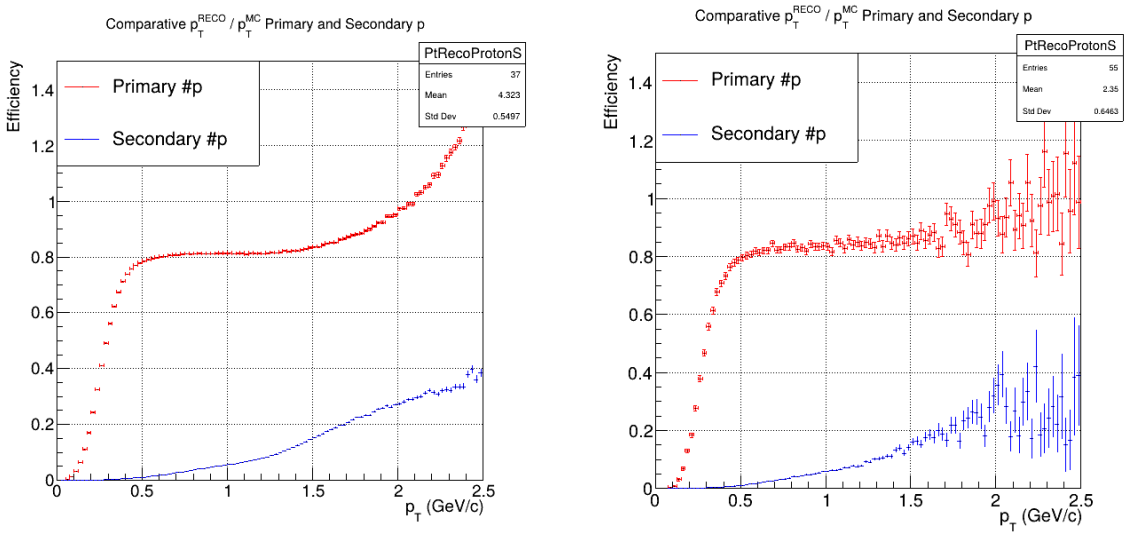

(a) The Δp_T with cut in Number of Hits. (b) The Δp_T with cut in η.

Figure 24: Comparative with and without cuts of the Δp_T.

In the graph of distributions for protons, it is evident that what is happening with secondary particles in both cases needs to be carefully examined. Although they exhibit similar behavior, the trend is somewhat unusual. The next subsection will analyze what is happening.

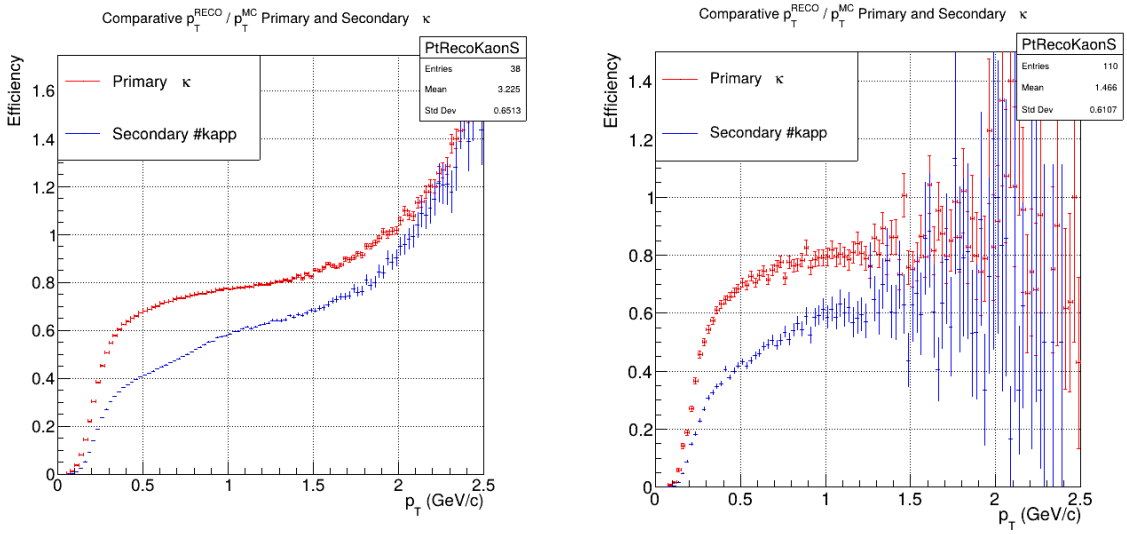

(a) The Δp_T with cut in Number of Hits. (b) The Δp_T with cut in η.

Figure 25: Comparative with and without cuts of the Δp_T.

To conclude this part, it is clear that in all comparisons of transverse momentum efficiency distributions, after 2, the information begins to have very high margins of error. This aligns with what was mentioned in the previous section when the histograms of transverse momentum resolution were examined.

5.8.1 What happened with the secondary protons?

To investigate what is happening with secondary protons, a histogram of the radius (horizontal axis) versus the reconstructed primary vertex in Z (vertical axis) was created. It shows that the vast majority of secondary protons are reconstructed at the edge of the detector, resulting in very few successful reconstructions.

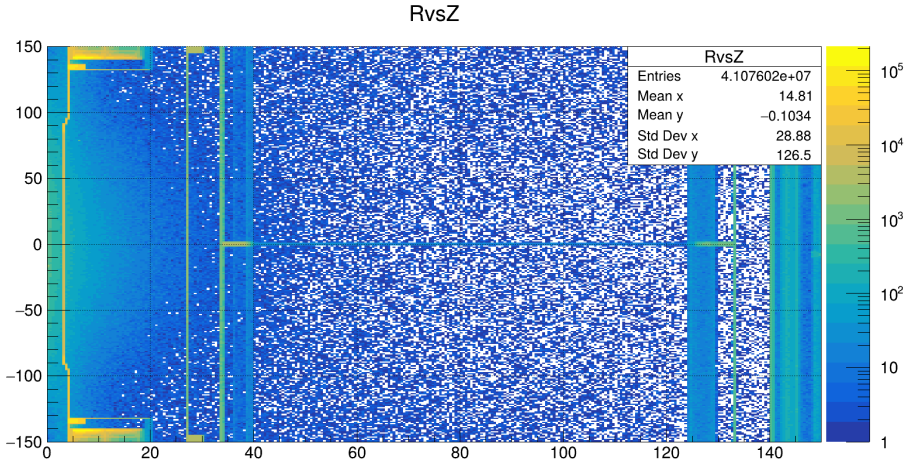

Figure 26: Comparative of Δp_T vs η with cuts Number of Hits and cut in η.

To address this, one approach could be to limit the primary vertex from which these secondary protons are reconstructed. Similarly, the same graphs could be created for pions and kaons, which is left for future work.

5.9 Resolution of Primary vertex versus Track Multiplicity

We also plotted the resolution of the primary vertex against track multiplicity, and both show similar trends.

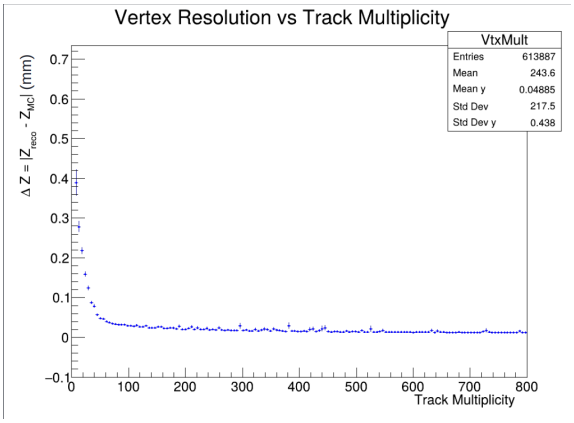

(a) Resolution of Primary vertex versus Track Multiplicity for Reduce Magnetic Field

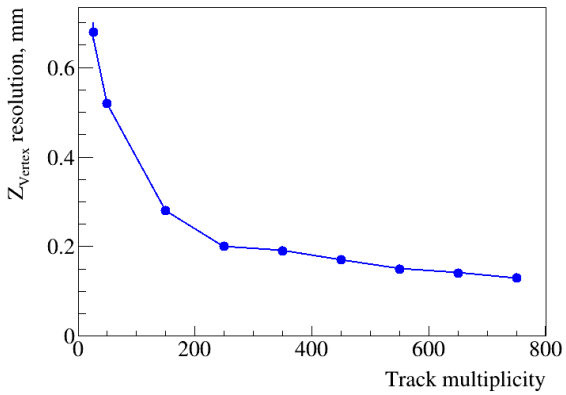

(b) Resolution of Primary vertex versus Track Multiplicity from [1]

Figure 27: Comparative of Resolution of Primary vertex versus Track Multiplicity.

6 Conclusions

In this report, we have detailed the process and methodology used to determine optimal cuts for analyzing transverse momentum resolution in the MPD experiment under reduced magnetic field conditions. We have evaluated various histograms and distributions to assess the efficiency of these cuts, focusing on parameters such as pseudorapidity and DCA Global. Our analysis has highlighted several key findings and areas for improvement.

We observed that the cuts for pseudorapidity and the number of hits show promising results in reducing errors, with a noticeable improvement in signal clarity and noise reduction. However, the results for DCA Global and the primary vertex position showed variability that requires further investigation. The differences between the reduced and full magnetic field conditions indicate that additional refinement is necessary to achieve optimal performance.

Given the complexity of the analysis and the constraints faced, it is clear that further work is needed. The next steps involve a more detailed examination of the secondary particles and a comprehensive comparison with existing data from similar studies. We plan to continue this work from Mexico, focusing on refining the cuts and optimizing the analysis.

The ongoing analysis will be conducted under the guidance of our advisors, with the goal of enhancing the precision and reliability of our results. We aim to integrate the insights gained from this report into future research and development efforts, ensuring that the findings contribute effectively to the broader objectives of the MPD experiment.

Overall, this report serves as a foundation for future improvements, and we are committed to advancing this research with continued diligence and expertise.

Acknowledgments

I thank Dr. Ivonne Maldonado for his advice, support and patience to teach me and help me in the development of this task, also for meetings and discussions outside the established times. I also thank Dr Vadim Kolesnikov and Natalia Kolomoyets for their contributions and advice, and willingness to answer questions.

Appendix A

Methodology

An account is requested in the cluster of the JINR and to find our class, you can follow the following address and the name is "*lowMgF*"[1]:

```
/scratch2/marquez/lowMgF
```

We started building our own class, read the class documentation of Dr Vitkar Kireyeu [2] to guide us in what we should do. We have been working with the class and created different macros that have helped us to develop each of the points of the task to be developed.

1 Running in the Offline Cluster

The data we want to analyze with the conditions we are looking for is too much information. It was necessary to make some adjustments in order to run all the information without having so many problems to run all the events without saturating the cluster or having some loss of information.

To start we had to divide our information into several lists. So, I chose to divided on many lists, folders and run to the offline cluster. Where each list have 1111 lines with 500 events.

Several macros were written and different commands were used to run all the lists in the offline cluster. For example, the macro "manyjobs.sh" is written and executed as follows.

```
source manyjobs.sh
```

Which its function is to create new folders and split our lists again and create new folders. Where apart from that the name of the test list will be changed in our file *"RunAnalyses. C"*, by the lists being created. Apart from this, our analysis train will be sent to the cluster.

```
sed -e "s/listTEST/x00/" RunAnalyses.C > dir${INDEX}/xa0/RunAnalyses.C

sed -e "s/listTEST/x01/" RunAnalyses.C > dir${INDEX}/xa1/RunAnalyses.C
```

The next part is just to send the runanauno file to the offline cluster with the command "sbatch".

[1]Likewise this can be found on GitHub:`https://github.com/iamaldonado/START_Summer24/tree/main/CarlosMarquez/lowMgF`

[2]You can check the documentation at the following link: `https://git.jinr.ru/nica/mpdroot/-/tree/dev/physics/nuclei?ref_type=heads`

```
sbatch runanauno
```

Once all this information has been created and run. We will have to join all our output files with a new macro, which is called *"mezcla. C"*. This gives us the following information.

```
[in]    root mezcla.C

[out]   tasklowMgFAll.root
```

Where the output file with the information of the 10 million events is *"tasklowMgFAll.root"*. Once you have this file, we can see all our histograms. The output file name can be changed and it is recommended to change it every time you use it. Otherwise you will be rewriting the output file.

If you want to know in detail how to run many files on the cluster offline, you can consult GitHub [3]. There is a more effective method, which we do not implement for time. However, it will be learned for future implementation [4].

2 Our Class

As mentioned above, a class was written with the name *"lowMgF"*. The purpose of this class is only to study and verify where cuts can be made to improve efficiency in the study of Collider Mode with reduced magnetic field. However, it is also used to replicate the cuts already known for the full magnetic field.

It is important to mention that there were some problems at the beginning, however we have managed to build a class that meets all the requirements to be able to successfully perform the task of the START program. Of course the code has been constantly modified until we can have a final job. However, at the time of writing this report, it can be said that each line has been ordered and commented on and tried to explain. This helps us understand what each line does. However, we plan to continue this research. So over time will improve and optimize this class.

There are several parts that we would like to highlight and explain from the class. The parts that will be shown immediately are from the file *"lowMgF.cxx"*. They will also mention in which lines are located, since if the reader wants to review them, can go to consult them on GitHub [5].

The first part that is necessary to mention is where all the cuts are defined, these are in lines 258 to 263. Here you have to notice that it is outside of any loop. So by defining them there, we are defining it in the whole class.

```
//____Cuts___________________________________________________________________

  const Double_t CutNHits = 27;          // My cut: 27
  const Double_t CutEta = 1.5;           // My cut: -1.5 to 1.5.
  const Double_t CutDCA = 1;             // My cut: 1 cm
  const Double_t CutpT = 0.15;           // My cut: 0.15 cm
```

[3] This whole procedure has been detailed and explained in detail on GitHub: `https://github.com/iamaldonado/START_Summer24/tree/main/CarlosMarquez/RunOffCluster`

[4] The documentation can be checked at the following link: `https://git.jinr.ru/nica_modules/mpd_scheduler/-/blob/dev/README.md`

[5] You can find the *lowMgF.cxx* file at the following link `https://github.com/iamaldonado/START_Summer24/blob/main/CarlosMarquez/lowMgF/lowMgF.cxx`

Here we can easily make a change to the full magnetic field cuts. This is useful to obtain information and thus compare the complete magnetic field against the reduced magnetic field.

```
//____Cuts_____________________________________________________________________

  const Double_t CutNHits = 27;          // My cut: 27
  const Double_t CutEta = 1.5;           // My cut: -1.5 to 1.5.
  const Double_t CutDCA = 1;             // My cut: 1 cm
  const Double_t CutpT = 0.15;           // My cut: 0.15 cm
```

Another aspect that is important to mention is that we define several variables outside of any loop, it is everything related to the primary vertex. We can check this out on lines 222 to 232.

```
        //Primary Vertex point
  Int_t nVert           = vtxs->GetEntriesFast();
  MpdVertex *vtx        = (MpdVertex*) vtxs->First();

  Double_t ZReco        = vtx -> GetZ();
  Int_t nTVert          = vtx->GetNTracks();
  Double_t ZMC          = mMCEventHeader-> GetZ();
  Double_t b            = mMCEventHeader -> GetB();
  Double_t absZ         = TMath::Abs( ZReco );

  Double_t DZ           = TMath::Abs( ZReco - ZMC );

  TVector3 Prim_Vtx(vtx->GetX(),vtx->GetY(),vtx->GetZ());
```

Similarly, everything related to these variables and their respective histograms were filled out in the same way outside of any loop.

However, it should be mentioned that for the multiplicity, it was likewise defined outside of any loop, as seen in lines 253 to 256.

```
        // Multiplicity
  Int_t refMult;

  refMult = 0;
```

However, the part where multiplicity is advancing in events if it goes into the first loop. Otherwise no event would be counted. We can find it in the lines 317 to 318.

```
        //Multiplicity
  refMult++;
```

Another important aspect to consider is that it is made two loops in the code. One is for the rebuilt part and another is for the Monte Carlo. The first loop of the reconstructed starts on lines 284 to 286. It ends on line 454.

```
// The main reco loop
  int ntr   = mKalmanTracks -> GetEntries();
  for (long int i = 0; i < ntr; i++) {
  ...
  } // Close the first loop.
```

In the part of the reconstructed loop more things were defined that helped us to perform the complete analysis. However, it will not be mentioned here because it is already commented on in the code.

The second loop, is only for the part of the Monte Carlo and starts in the lines 459 to 461. It ends in the line 488.

```
Int_t nmctracks = mMCTracks->GetEntriesFast();

for (int i=0; i<nmctracks; i++){
...
} // Close the second loop.
```

Bibliography

[1] Abgaryan, V. et al. (MPD Collaboration) *Status and initial physics performance studies of the MPD experiment at NICA.* Eur. Phys. J. A (2022) 58, 140.

[2] Buša Jr, J., Hnatič1, S., Rogachevsky, O.V. (2021). *PERFORMANCE ANALYSIS AND OPTIMIZATION OF MPDROOT* Revised 22 August 2024, at https://ceur-ws.org/Vol-3041/75-79-paper-13.pdf

[3] Jlzhang. (2017). *2009 Lambda DLL @ 200 GeV | The STAR experiment.* Revised 22 August 2024, at https://drupal.star.bnl.gov/STAR/pwg/spinAnalysisStatus.html/2009-lambda-dll-200-gev

[4] Kekelidze V.D. et al. *Three stages of the NICA accelerator complex.* Eur. Phys. J. A (2016) 52, 211.

[5] Lechner, A. *Particle Interations with Matter.* CERN Document Server. Retrieved April 17th, 2024, from https://cds.cern.ch/record/2674116/files/660.pdf

[6] MPD experiment – another step forward. (s.f.). *Joint Institute For Nuclear Research.* Retrieved April 17, 2024, from https://www.jinr.ru/posts/mpd-experiment-another-step-forward/

[7] MPDROOT Developers. (s.f.). *MpdTrack.h.* MPDROOT. Retrieved April 14th, 2024, from https://git.jinr.ru/nica/mpdroot/-/blob/dev/core/mpdBase/MpdTrack.h?ref_type=heads

[8] MPDROOT Developers. (s.f.). *MPDROOT Repository.* MPDROOT. Retrieved 17 April 2024, from https://git.jinr.ru/nica/mpdroot/-/tree/v23.12.23?ref_type=tags

[9] Multi purpose detector: the Mega-Science Project «NICA». (2024). Retrieved April 17th, 2024, from https://mpd.jinr.ru/

[10] NICA - Nuclotron-based Ion Collider FAcility. (s.f.). *Collider.* GitHub. Retrieved 22 August 2024, from https://nica.jinr.ru/projects/collider.php

[11] NICA - Nuclotron-based Ion Collider FAcility. (s.f.). *Time projection chamber.* Retrieved 22 August 2024 https://nica.jinr.ru/projects/mpd.php

[12] Raghunath Sahoo. *Relativistic Kinematics.* E-print: 1604.02651 [nucl-ex] https://arxiv.org/pdf/1604.02651.pdf